Australian Government
Geoscience Australia
Exploring for the Future

Thermomechanical models of the Australian plate

M. J. Hoggard[1], J. Hazzard[2], Z. Sudholz [1,3], F. Richards [2], T. Duvernay [1], J. Austermann [4], A. L. Jaques [1], G. Yaxley [1] and K. Czarnota[5]

[1]Australian National University, [2]Imperial College London, [3]University of Cambridge, [4]Columbia University, [5]Geoscience Australia

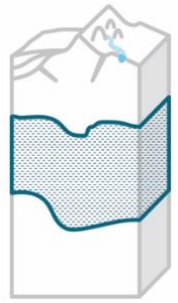

Abstract. The thickness and thermal structure of continental lithosphere influences the location of seismic and volcanic hazards and is important for predicting long-term evolution of landscapes, sedimentary basins, and the distribution of natural resources. In this project, we have developed new, continental-scale models of the thermomechanical structure of the Australian plate. We begin by compiling an inventory of >9000 geochemical analyses of peridotitic xenoliths and xenocrysts from across the continent that have been carried up to the surface in volcanic eruptions. We apply thermobarometric techniques to constrain their pressure and temperature of equilibration and perform steady-state heat flow modelling to assess the paleogeotherm beneath these sites. We subsequently use the paleogeotherms as constraints in a Bayesian calibration of anelasticity at seismic frequencies to provide a mapping between seismic velocity and temperature as a function of pressure. We apply this method to several regional-scale seismic tomography models, allowing the temperature and steady-state diffusion creep viscosity to be continuously mapped throughout the Australian lithospheric and asthenospheric mantle. Our models include assessment of uncertainties and can be used to query thermomechanical properties, such as lithospheric thickness and heat flow through the Moho.

It is increasingly recognised that the thermomechanical properties of continental lithosphere play a fundamental role in modulating geological processes across a range of spatiotemporal scales. Lithospheric thickness has been linked, for example, to seismogenic thickness and variations in the frequency and magnitude of seismicity (Craig et al. 2011), long-term active tectonics and the style of intraplate deformation (Liu & Zoback 1997), sedimentary basin geometries (Ebinger et al. 2019), and surface heat flow (Hyndman et al. 2005). The rigid plate acts as a lid that profoundly interacts with the underlying asthenosphere, limiting the shallowest levels of decompression melting above mantle plumes and localising volcanism associated with shear-driven upwelling (Niu et al, 2011; Davies & Rawlinson 2014; Duvernay et al. 2021; Niu, 2021). Thick areas of lithospheric mantle (known as *cratons*) enhance the preservation potential of surface rocks, providing a vestige for areas of Earth's oldest continental crust and providing geodynamic conditions that are optimal for the generation of giant mineral deposits (Jordan 1978; Griffin et al. 2013; Skirrow et al. 2018; Hoggard et al. 2020). To better understand the geodynamic setting of the Australian plate and its influence on surface processes and the distribution of natural resources, it is desirable to develop models of its thermomechanical structure, which has been the general goal of this extensive collaboration.

Defining the lithosphere

From a compositional perspective, lithosphere is composed of two main layers - crust and mantle. Continental crust is formed from crystallised, mantle-derived melts that are buoyant and enriched in incompatible elements, including the radiogenic heat producing uranium, thorium and potassium (Jaupart & Mareschal 2003). The lithospheric mantle is peridotitic (i.e. composed of magnesium-rich silicates) and parts of it, particularly in cratonic regions, are thought to be the residuum leftover from melt extraction early in Earth's history (Jordan 1978). It is considerably denser than crustal rocks, but in places more buoyant than the underlying convecting mantle. It owes it greater buoyancy to the fact that it is more refractory and mostly more dehydrated than the underlying mantle. It is also depleted in radiogenic elements and therefore has minimal internal heat production.

From a thermomechanical perspective, a vertical column through continental lithosphere is divided into three distinct domains (Turcotte & Schubert 2002; Figure 1). First, the layer nearest to the surface, where temperatures are lowest, is known as the *mechanical boundary layer* (MBL). It consists of the crust and upper portion of lithospheric mantle. The MBL is

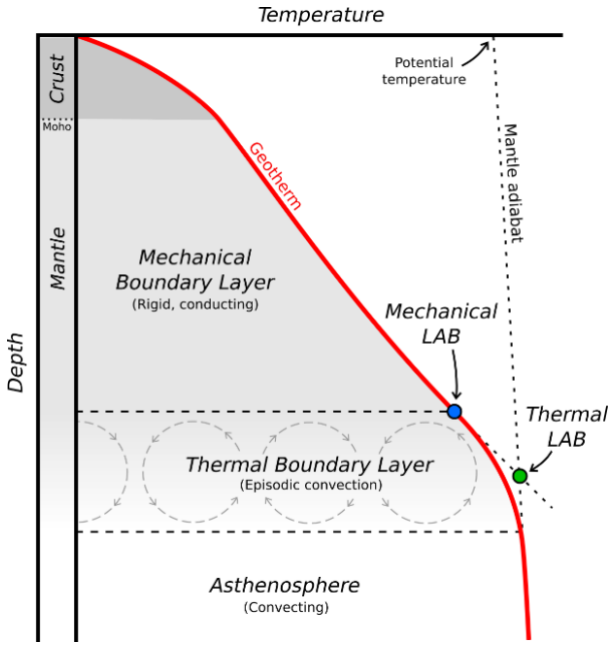

Figure 1: *Schematic cartoon of the fundamental layers making up continental lithosphere. Red line = steady-state geotherm; blue and green circles = definition of mechanical and thermal lithosphere-asthenosphere boundary (LAB), respectively.*

mechanically rigid and does not actively participate in convection. Heat passing through the MBL therefore does so by conduction, with typical temperature gradients of 15-35°C/km dependent on MBL thickness and crustal radiogenic heat production. The second domain is called the *thermal boundary layer* (TBL). Due to higher temperatures, the TBL is not mechanically rigid over geological timescales and undergoes episodic destabilisation and small-scale convection. It therefore possesses a temperature profile that transitions from fully conductive in the overlying MBL to fully adiabatic in the underlying convecting mantle. The top of the convecting mantle is known as the *asthenosphere* and makes up the third domain. It is characterised by adiabatic temperature gradients of 0.4-0.6°C/km. Projecting the mantle adiabat up to the surface defines the *potential temperature*, which has a global average of ~1330°C but can locally vary by as much as ±100°C.

Paleogeotherm inventory

One of the strongest constraints on lithospheric structure comes from direct samples of the mantle that are brought to the surface by volcanic eruptions. Known as *xenoliths* (or *xenocrysts* if they are only single mineral grains), the petrology and geochemistry of these samples can be used to constrain local temperature structure and lithological architecture (e.g. O'Reilly & Griffin 1985). Growing databases of such mantle xenoliths and xenocrysts (driven, in part, by extensive exploration for diamonds) have accompanied the calibration of robust thermobarometers that exploit chemical exchanges between constituent minerals to constrain their temperature and pressure of equilibration (e.g. Nimis & Grutter 2010).

Here, we have undertaken a comprehensive reassessment of available xenolith and xenocryst occurrences throughout the continent. As well as digitising data from academic literature stretching back to the 1960s, we have supplemented with our own new analyses performed at the Centre for Advanced Microscopy, Australian National University. The final database consists of over 9000 constraints on the major elemental oxides of mantle minerals, predominantly clinopyroxene and garnet, but also some orthopyroxene, olivine and spinel. These come from 60 different sites that are fairly well distributed across the continent, although central Australia is under-represented (Figure 2a). They include samples associated with kimberlite and ultramafic lamprophyre occurrences in the Kimberley, Yilgarn, Gawler and North Australian Cratons, and Jurassic-to-Neogene mafic volcanism throughout the Tasmanides (stretching north-to-south across eastern Queensland, New South Wales, Victoria and into Tasmania, see also Sudholz et al., this volume).

We have applied published thermobarometric relationships to obtain equilibration pressure, P, and temperature, T. Geochemical analyses were initially screened for quality using common protocols, before being assessed with two different thermobarometer pairings. For xenoliths that have analyses on co-existing clinopyroxene, orthopyroxene and garnet, we use the thermometer from Taylor (1998) that exploits the exchange of calcium and magnesium between clinopyroxene and orthopyroxene in combination with the barometer of Nickel & Green (1985) that is based on aluminium exchange between orthopyroxene and garnet. For the single-grain clinopyroxenes, we use the chrome-diopside thermometer of Nimis & Taylor (2000) and barometer of Sudholz et al (2021). This thermobarometer pairing relies on the diopside having co-existed with orthopyroxene and garnet in the original assemblage and will give spurious results for clinopyroxene grains that originate from spinel peridotites. Each suite of estimated P-T points was visually inspected, and any obvious outliers culled. The values typically fall along a broadly consistent linear array, although sometimes are split into a shallower and deeper population with conspicuous absence of diopsides from mid-lithospheric depths (Figure 2b). Localities that are in close proximity to one another generally exhibit consistent P-T arrays and have therefore been combined into a single paleogeotherm. Further details and other examples are given in the accompanying paper by Sudholtz et al. (this volume).

Paleogeotherm modelling has been performed at each of these sites using FITPLOT by minimising misfit between each individual P-T array and a steady-state geotherm, whereby the heat flow into any point from below plus internal radiogenic heat production is balanced by heat conducting out to shallower depths (Mather et al. 2011). Application to our dataset yields 32 usable paleogeotherms, of which we classify 27 to be of sufficiently high reliability to be of use in constructing the full thermomechanical model. We suspect that the other five are probably also reliable but have omitted them from further use due to factors such as only returning P-T values from shallower than 30 km and/or relying on only a single P-T constraint. The mechanical LAB estimates here are slightly shallower (~10-15%, equivalent to ~10-30 km) than the thermal LAB estimates presented in Sudholtz et al. (2022, 2023a,b).

Six representative paleogeotherms are shown in Figure 2b. To briefly summarise our results, the lithosphere is relatively thick beneath the Yilgarn Craton, with Melita and Jewill returning mechanical LAB depths of ~160-180 km. Northwest of the Yilgarn in the Carnarvon Basin, Wandagee returns a mechanical LAB closer to ~145 km. Webb in central Australia's Arunta province is substantially thinner, yielding ~120 km (Sudholtz et al., 2023), while paleogeotherms from the Kimberley Craton in northern West Australia consistently infer very thick lithosphere. Data from Ashmore, Argyle, Calwynyardah, and Ellendale are all broadly consistent with the same paleogeotherm, yielding a mechanical LAB of 175-190 km. This result is interesting since Argyle was emplaced at 1257 ± 15 Ma (Olierook et al., 2023), Ashmore at ~800 Ma and Calwynyardah and Ellendale date from early Miocene times (Phillips et al., 2022). Thus, for at least a billion years, the lithosphere beneath the Kimberley Craton appears to have been relatively stable (Jaques et al., 2018; Hoggard et al., 2020; Sudholtz et al. 2023). Continuing eastwards into the Northern Territory, Timber Creek sits on the margin of the Proterozoic Birrindudu Basin and returns a well-defined P-T array that yields a surprisingly shallow mechanical LAB of ~80 km. This depth contrasts with a value of 190 km from Merlin further east on the edge of the Proterozoic McArthur Basin. In the Gawler Craton of South Australia, Mount Hope, El Alamein and Orroroo all return consistent results and a mechanical LAB at 165-170 km depth (with the thermal LAB estimated at 190-205 km extending to ~220 km in the deepest sections near Euralia and Port Augusta: Sudholtz et al. 2022) This inter-site agreement lends weight to them providing an accurate representation of lithospheric structure in the central Gawler and they mark the start of a gradual thinning of the lithosphere towards the east. Immediately to the east, data from the Terrowie Cluster include a number of kimberlite fields and indicates a mechanical LAB depth of 125-135 km. Continuing eastwards across the Curnamona province and into western New South Wales, the paleogeotherms from Kayrunnera and Dolo Hill both record consistent mechanical LAB depths of 115-120 km.

Paleogeotherms from the Tasmanides are in marked contrast to everything further west, consistently indicating that the lithosphere is substantially thinner here. Starting in northern Queensland, Cone 32, Sapphire Hill and Bachelor Crater yield some of the shallowest mechanical LAB depths of 50-60 km and geotherms that make a close approach to

the dry solidus in the TBL - a result that is consistent with their 1 Ma or younger emplacement ages. Scrubby Hill, Sheep Station Knob, Boowinda Creek and Brigooda have slightly deeper values (reaching ~70 km) that are broadly consistent with one another, which is encouraging given that Scrubby Hill and Boowinda Creek each rely on only a single P-T constraint. Continuing southwards over the border into New South Wales, Ruby Hill, Gloucester and Abercrombie similarly have only a few P-T data but yield mechanical LAB depths of 60 km, 70 km and 75 km, respectively, potentially hinting at gradual thickening of the lithosphere southwards. That pattern is consistent with the more extensive data from Jugiong and the Eucumbene-Tumut water tunnel (immediately northwest of the Australian Capital Territory), which indicate a mechanical LAB at 75 km. P-T constraints from Delegate and nearby Monaro are consistent with one another (although the Monaro array is less well defined) and yield ~65 km, which is interesting given the difference in their respective emplacement ages of 170 ± 5 Ma and 45 ± 11 Ma. Continuing into Victoria, both Mount Anakie and Bullenmerri record thin lithosphere (mechanical LABs of 60 km and 50 km, respectively) with geotherms that approach and in some cases cross the dry solidus, matching expectations from their <1 Ma eruption ages. Finally, lithosphere is slightly thicker beneath Tasmania, with Table Cape yielding a mechanical LAB at 60 km and Bow Hill closer to 70 km.

Anelastic calibration

Thermobarometric analysis of mantle xenoliths and xenocrysts provides a means of directly constraining the continental geotherm underlying the site of their eruption. These paleogeotherms are, however, spottily distributed throughout the continent and are therefore of limited use for constraining lithospheric structure at regional scales. Seismic tomography models, on the other hand, provide laterally continuous information. Nevertheless, they provide measurements of seismic velocity, which is a derivative property of the underlying temperature structure. It is therefore necessary to convert seismic velocity variations into temperature if we are to use them to infer lithospheric structure.

The speed at which seismic energy travels through mantle rocks is strongly dependent upon their temperature. At temperatures less than 90% of the melting temperature, energy transfer occurs via minute displacements of the mineral lattice and surrounding grain boundaries that is predominantly accommodated by elastic strain. Laboratory studies have shown that the bulk and shear moduli that control this elastic deformation have an approximately linear dependence on temperature and pressure, such that seismic velocities steadily increase as the temperature reduces and/or pressure increases. This regime is known as variations in the *anharmonic velocity*.

When temperatures rise above the 90% of melting temperature threshold, an additional mechanism of deformation starts to occur, known as *anelasticity*. In this regime, strain of the material starts to become time-dependent in response to stress (rather than instantaneous, as in the elastic case), although it remains fully recoverable once the driving stress is removed. The effect of anelasticity is that, as temperatures continue to increase, seismic velocities drop away faster than would be expected from the anharmonic relationship. Given that temperatures within the shallow asthenosphere can come well within the 90% threshold (and indeed must cross the solidus to generate the Neogene basaltic melts found throughout much of eastern Australia), it is essential to account for anelasticity when using seismic velocity variations to construct a robust temperature model of the Australian upper mantle.

In this project, we have used the “pre-melting” YT16 anelasticity formulation of Yamauchi & Takei (2016), which contains seven material parameters that are not known a priori for the mantle. We have elected to use a recently developed Bayesian inversion scheme (Hazzard et al. 2023) to calibrate these parameters by evaluating the fit between temperatures obtained from the paleogeotherm analysis with those derived from conversion of seismic velocity-to-temperature at the same localities. For the seismic tomography, we have assessed two published regional

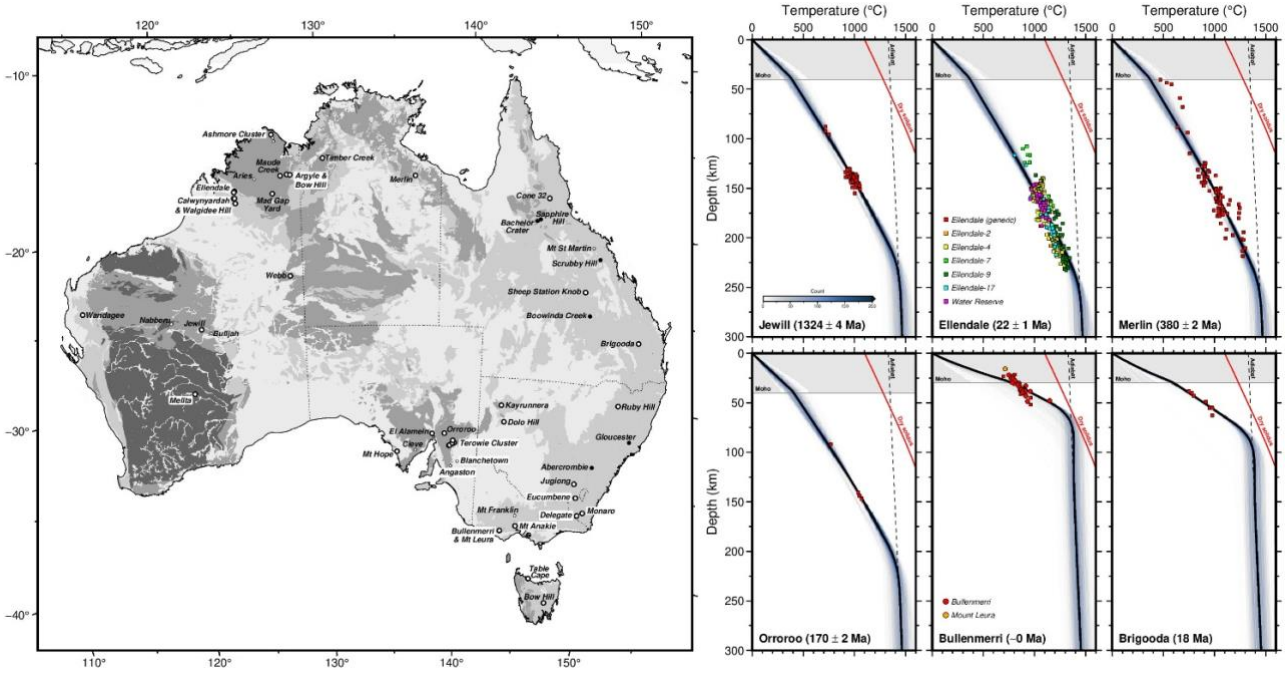

Figure 2: *Localities of mantle xenolith and xenocryst occurrences compiled in this study and representative paleogeotherms labelled with emplacement ages. Dark/medium/light/white polygons = approximate extent of Archean/Proterozoic/Paleozoic plus Mesozoic. Material from multiple pipes in the same vicinity have been grouped (see individual legends).*

models that cover the Australian continent and include large numbers of surface waves. These waves are confined to the upper few 100 km of the Earth and are therefore excellent for imaging lithospheric structure. The first, FR12 (Fishwick & Rawlinson, 2012), is selected due to the extensive manual quality-checking of waveforms that was performed during its construction and therefore, despite being over a decade old, its input data is of exceptionally high quality. The seismometer network used in its construction consisted of a combination of temporary array deployments and permanent stations, resulting in >13,000 individual source-to-receiver paths and one of the best currently available ray-path coverages across the continent. The second, Aus22 (de Laat et al. 2023), is one of the most recent regional studies from the Australian plate and therefore benefits from a high level of coverage by ray paths and up-to-date techniques for inversion of seismic velocities.

The results of our anelastic calibration of material parameters are shown in Figure 3. We focus on FR12 throughout the rest of this abstract, but equivalent results for Aus22 are also available. As a general rule, we find that the posterior distribution is a relatively smooth function with clear optimal parameter value in the vicinity of the maximum a posteriori model. The two parameters that least well obey this behaviour are the diffusion creep activation energy, Ea, which shows two additional groupings at low values, and the solidus gradient, dTs/dz, which returns a spread of outlier values extending above ~1.5°C/km. In terms of trade-offs, there is a distinct covariation between μ0, dμ/dT and dμ/dP, which are parameters controlling the anharmonic velocity as a function of pressure and temperature and has been previously recognised (Hazzard et al. 2023). The other trade-off occurs between Ea and the reference viscosity, eta, which control the strength of the anelastic deformation process.

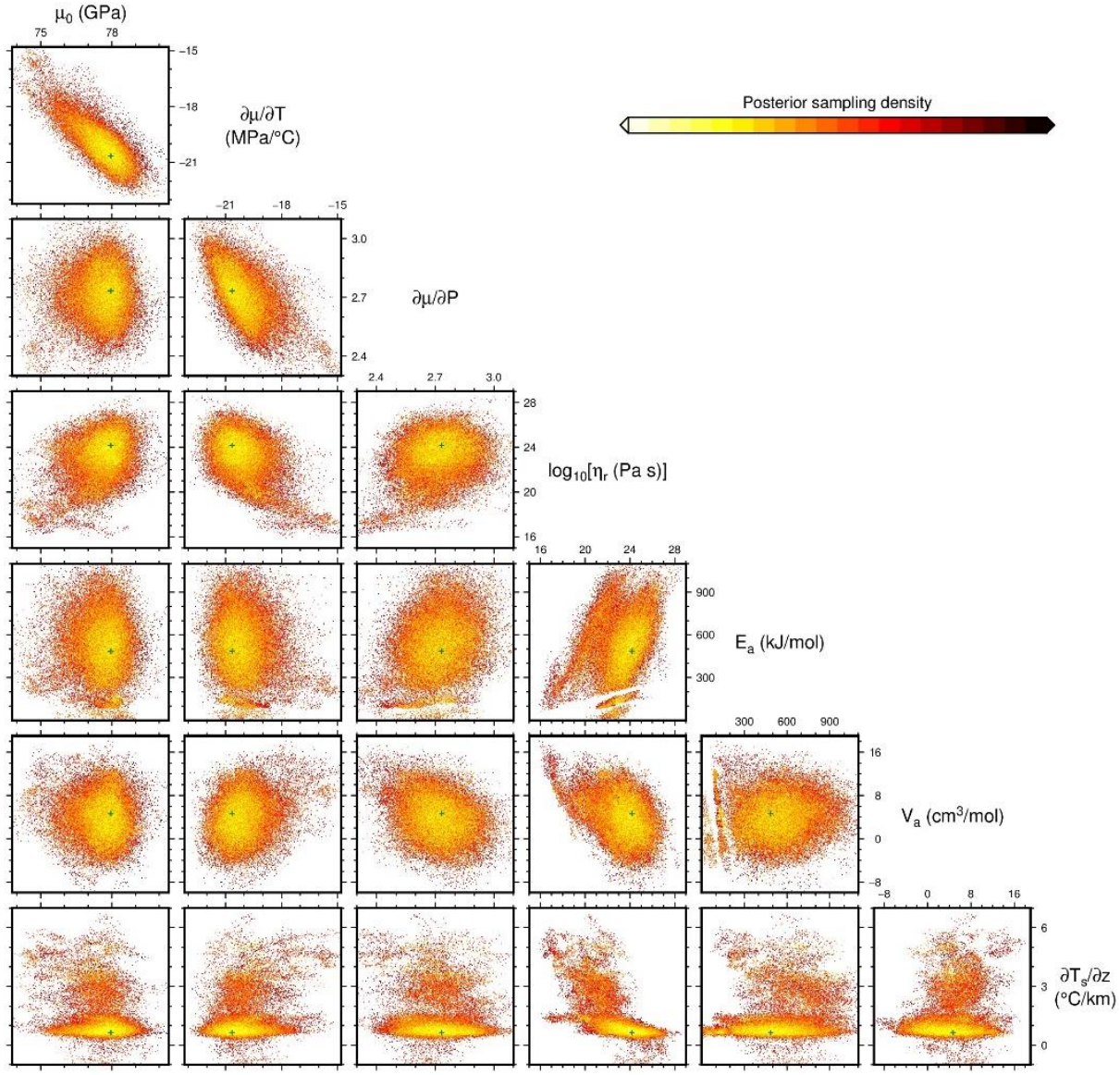

Figure 3: *Posterior distributions and trade-offs between the seven calibrated anelasticity parameters for FR12 tomography model. Points = 200,000 individual samples, coloured by posterior sampling density; green cross = maximum a posteriori model.*

Final temperature model

Armed with a calibrated anelasticity parameterisation, we can convert seismic velocity variations into temperature throughout the domain of the seismic tomography model. The final processing step in our workflow is to account for the fact that these seismically inferred temperatures are not

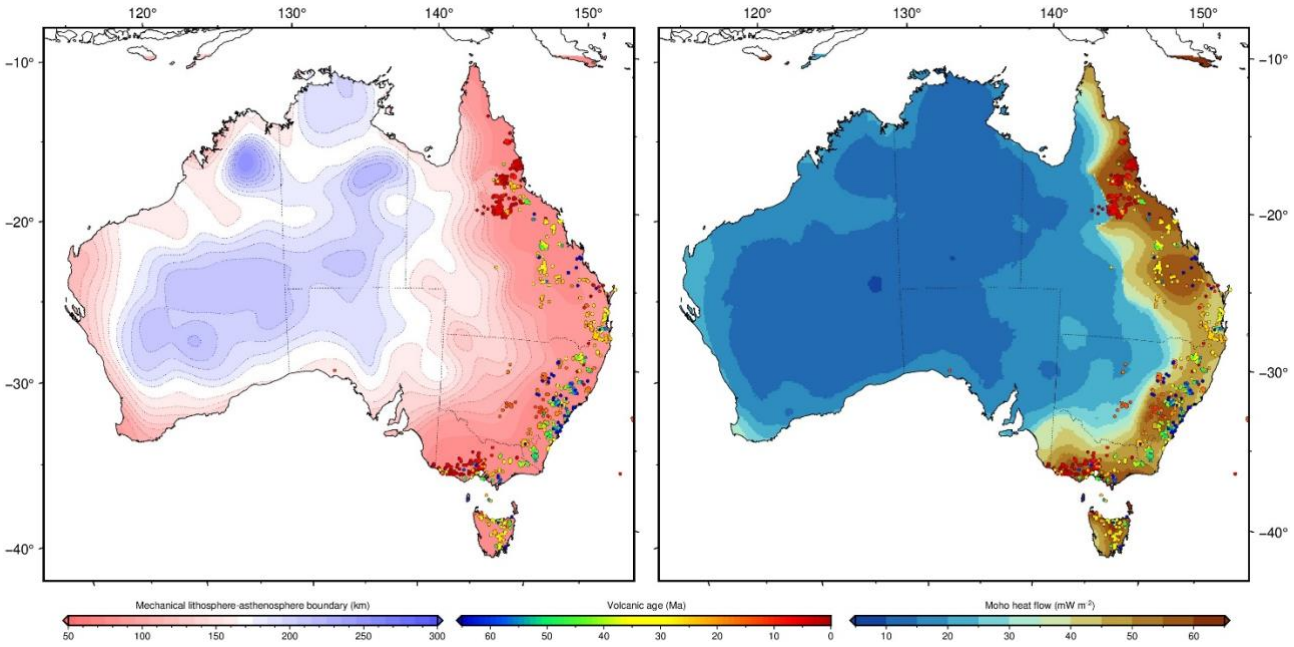

Figure 4: *Predicted mechanical LAB depth and Moho heat flow overlain with locations of Cenozoic volcanism, coloured by eruption age.*

necessarily fully consistent with conductive heat flow in the MBL. For example, underestimation of crustal thickness during construction of the seismic tomography model results in downward bleeding of crustal velocities into the underlying mantle, which are subsequently erroneously converted into hot temperatures at shallow depths. We therefore fit a steady-state geotherm to the temperature estimates and use it to fix the temperature in regions that are affected by such anomalies. The final model consists of estimates of temperature, thermal conductivity and steady-state diffusion creep viscosity as a function of location and depth throughout the Australian upper mantle.

Using this model, we can query a number of different properties of interest. For example, Figure 4a shows the depth to the 1175°C isothermal surface, which is a proxy for the average thickness of the MBL, while Figure 4b shows the expected heat flow through the Moho. Overlaying these two fields with the distribution of Cenozoic volcanic rocks throughout the continent, it is immediately apparent that volcanism is both confined to regions of thin lithosphere and that the youngest volcanism in Queensland and Victoria occurs in regions with some of the highest heat flow through the Moho. Other uses for the model include estimating the Curie depth (i.e. the depth-extent of ferromagmetism), the temperature component of electrical conductivity anomalies (thereby permitting isolation of features related to compositional variations in magnetotelluric studies) and constraining viscoelastic models of surface motion and sea-level change due to melting of ice sheets and glacial isostatic adjustment. Since cratonic lithosphere is inexorably linked to the genesis of many different classes of mineral deposit (e.g. Griffin et al. 2013; Skirrow et al. 2018; Hoggard et al. 2020), these models also underpin mineral exploration efforts, particularly as continuous maps of lithospheric structure allow the identification of prospective domains, even in regions that are undercover. The three-dimensional thermomechanical models derived from FR12 and Aus22 are publicly available from Geoscience Australia's data portal and include the propagation of uncertainty in anelasticity parameters into the final model.

References

Craig, T. J., J. A. Jackson, K. Priestley, & D. P. McKenzie (2011). Earthquake distribution patterns in Africa: Their relationship to variations in lithospheric and geological structure, and their rheological implications. Geophysical Journal International, 185, 403–434.

Davies, D. R. & N. Rawlinson (2014). On the origin of recent intraplate volcanism in Australia. Geology, 42 (12), 1031–1034.

Duvernay, T., D. R. Davies, C. R. Mathews, A. H. Gibson, & S. C. Kramer (2021). Linking intraplate volcanism to lithospheric structure and asthenospheric flow. Geochemistry, Geophysics, Geosystems, 22 (8), e2021GC009953.

Ebinger, C. J., S. J. Oliva, T. Q. Pham, K. Peterson, et al. (2019). Kinematics of active deformation in the Malawi Rift and Rungwe Volcanic Province, Africa. Geochemistry, Geophysics, Geosystems, 20 (8), 3928–3951.

Griffin, W. L., G. C. Begg, & S. Y. O'Reilly (2013). Continental-root control on the genesis of magmatic ore deposits. Nature Geoscience, 6, 905–910.

Hazzard, J. A. N., F. D. Richards, S. D. B. Goes, & G. G. Roberts (2023). Probabilistic assessment of Antarctic thermomechanical structure: Impacts on ice sheet stability. Journal of Geophysical Research: Solid Earth, 128, e2023JB026653.

Hoggard, M. J., K. Czarnota, F. D. Richards, D. L. Huston, A. L. Jaques, & S. Ghelichkhan (2020). Global distribution of sediment-hosted metals controlled by craton edge stability. Nature Geoscience, 13, 504–510.

Hyndman, R. D., C. A. Currie, & S. P. Mazzotti (2005). Subduction zone backarcs, mobile belts, and orogenic heat. GSA Today, 15 (2), 4–10.

Jaques, A.L., Luguet, A., Smith, C.B., Pearson, D., Yaxley, G.M., Kobussen, A., (2018). Nature of the mantle beneath the Argyle AK1 lamproite pipe: Constraints from mantle xenoliths, diamonds, and lamproite geochemistry. In: Davy, T., et al. (Eds.),

Geoscience and Exploration of the Argyle, Bunder, Diavik, and Murowa Diamond Deposits. Society of Economic Geologists Special Publication 20, pp. 119–143

Jaupart, C. & J.-C. Mareschal (2003). Constraints on crustal heat production from heat flow data. In: Treatise on Geochemistry, Volume 3 (edited by R. L. Rudnick), chap. 3.02, pp. 65–84. Elsevier.

Jordan, T. H. (1978). Composition and development of the continental tectosphere. Nature, 274, 544–548.

Liu, L. & M. D. Zoback (1997). Lithospheric strength and intraplate seismicity in the New Madrid seismic zone. Tectonics, 16 (4), 585–595.

Mather, K. A., D. G. Pearson, D. P. McKenzie, B. A. Kjarsgaard, & K. Priestley (2011). Constraints on the depth and thermal history of cratonic lithosphere from peridotite xenoliths, xenocrysts and seismology. Lithos, 125, 729–742.

Nickel, K. G. & D. H. Green (1985). Empirical geothermobarometry for garnet peridotites and implications for the nature of the lithosphere, kimberlites and diamonds. Earth and Planetary Science Letters, 73, 158–170.

Nimis, P. & H. Grütter (2010). Internally consistent geothermometers for garnet peridotites and pyroxenites. Contributions to Mineralogy and Petrology, 159, 411–427.

Nimis, P. & W. R. Taylor (2000). Single clinopyroxene thermobarometry for garnet peridotites. Part I. Calibration and testing of a Cr-in-Cpx barometer and an enstatite-in-Cpx thermometer. Contributions to Mineralogy and Petrology, 139, 541–554.

Niu, Y. (2021). Lithosphere thickness controls the extent of mantle melting, depth of melt extraction and basalt compositions in all tectonic settings on Earth – A review and new perspectives. Earth-Science Reviews, 217, 103614

Niu, Y.L., Wilson, M., Humphreys, E.R., O'Hara, M.J., 2011. The origin of intra-plate ocean island basalts (OIB): the lid effect and its geodynamic implications. Journal of Petrology, 52, 1443–1468.

Olierook, H.K.H., Fougerouse, D., Doucet, L.S. et al. Emplacement of the Argyle diamond deposit into an ancient rift zone triggered by supercontinent breakup. Nature Communications 14, 5274 (2023). https://doi.org/10.1038/s41467-023-40904-8

O'Reilly, S. Y. & W. L. Griffin (1985). A xenolith-derived geotherm for southeastern Australia and its geophysical implications. Tectonophysics, 111, 41–63.

Phillips, D., Clarke, W. & Jaques, A.L. (2022). Age and origin of the West Kimberley lamproites, Western Australia, Lithos, 432–433, 106913.

Skirrow, R. G., S. E. van der Wielen, D. C. Champion, K. Czarnota, & S. Thiel (2018). Lithospheric architecture and mantle metasomatism linked to Iron Oxide Cu-Au ore formation: Multidisciplinary evidence from the Olympic Dam region, South Australia. Geochemistry, Geophysics, Geosystems, 19, 2673–2705.

Sudholz, Z.J., Reddicliffe, T.H., Jaques, A.L., Yaxley, G.M., Haynes, M., Gorbatov, A., Czarnota, K., Frigo, C., Maas, R. and Knowles, B., 2023a. Petrology, age, and rift origin of ultramafic lamprophyres (aillikites) at Mount Webb, a new alkaline province in Central Australia. Geochemistry, Geophysics, Geosystems, 24(10), p.e2023GC011120.

Sudholz, Z.J., Jaques, A.L., Yaxley, G.M., Taylor, W.R., Czarnota, K., Haynes, M.W., Frewer, L., Ramsay, R.R., Downes, P.J. and Cooper, S.A., 2023b. Mapping the structure and metasomatic enrichment of the lithospheric mantle beneath the Kimberley Craton, Western Australia. Geochemistry, Geophysics, Geosystems, 24(9), p.e2023GC011040.

Sudholz, Z.J., Yaxley, G.M., Jaques, A.L., Cooper, S.A., Czarnota, K., Taylor, W.R., Chen, J. and Knowles, B.M., 2022. Multi-Stage Evolution of the South Australian Craton: Petrological Constraints on the Architecture, Lithology, and Geochemistry of the Lithospheric Mantle. Geochemistry, Geophysics, Geosystems, 23(11), p.e2022GC010558.

Sudholz, Z. J., G. M. Yaxley, A. L. Jaques, & G. P. Brey (2021). Experimental recalibration of the Cr-in-clinopyroxene geobarometer: Improved precision and reliability above 4.5 GPa. Contributions to Mineralogy and Petrology, 176 (11).

Sudholz, Z. J., G. M. Yaxley, A. L. Jaques, Czarnota, K & Haynes, M.W. (2024). Xenolith constraints on lithospheric architecture and mantle geochemistry of Australia. This publication.

Taylor, W. R. (1998). An experimental test of some geothermometer and geobarometer formulations for upper mantle peridotites with application to the thermobarometry of fertile lherzolite and garnet websterite. Neues Jahrbuch für Mineralogie - Abhandlungen, 172, 381–408.

Turcotte, D. L. & G. Schubert (2002). Geodynamics. Cambridge University Press, Cambridge, 2nd edn.

Yamauchi, H. & Y. Takei (2016). Polycrystal anelasticity at near-solidus temperatures. Journal of Geophysical Research: Solid Earth, 121 (11), 7790–7820.